# Directed Self-Assembly of Surfactants in Carbon Nanotube Materials

**Panagiotis Angelikopoulos and Henry Bock***

*Department of Chemical Engineering, Heriot-Watt University, Edinburgh, EH14 4AS, Scotland, United Kingdom*

*Received: June 03, 2008; Revised Manuscript Received: July 26, 2008*

The self-assembly of surfactant molecules on crossing carbon nanotubes has been investigated using a bead-spring model and implicit solvent dissipative particle dynamics simulations. Adsorption is directed to the nanotube crossing by its higher hydrophobic potential which is due to the presence of two surfaces. As a consequence of the tendency of surfactant molecules to self-assemble into micelles, the adsorbed molecules form a "central aggregate" at the crossing, thus, confining the molecules to the immediate vicinity of the crossing. Adsorption on the remaining nanotube surface becomes significant only at higher surfactant concentrations, where the molecules self-assemble to hemimicelles which grow continuously to full micelles upon increase of the (bulk) surfactant concentration. Our results allow two conclusions for the rational design of nanostructured materials: (i) the size of the central aggregate can not be much larger than that of a bulk micelle and (ii) control of the adsorbed structures is conveniently possible via the (bulk) surfactant concentration.

## I. Introduction

Because of their exceptional set of properties, carbon nanotubes (CNTs) have been proposed for a large range of applications ranging from high-strength materials usefull, e.g., as bone scaffolds to highly efficient and flexible field emitters and nanoelectronics. Although CNTs are central to all these applications, usually they are accompanied by other materials for structural or functional reasons.

For example, although individual nanotubes are strong, CNT materials are typically much weaker.[1−4] The weakest materials are those with a random arrangement of nanotubes such as sheets or papers.[5,6] Their weakness is caused by the "smoothness" of the CNTs, their weak mutual interaction, and the small contact area. Deposition of material, usually polymers, between the nanotubes can improve material strength significantly.[7,8]

Additives can also enhance function: for example, the selectivity of CNT sensors can be enhanced by coating the nanotubes with organic molecules.[9] This coating then acts as a filter letting only certain molecular species pass while blocking others. In CNT biosensors, on the other hand, the coating might be endowed with receptors making it part of the transducer.[10] Amphiphilic molecules are often used for coatings as they can be applied conveniently from solution.

In these applications as well as in many others involving CNTs or other nanoscale building blocks, it is essential that we can control the material's nanoscale structure, e.g., incomplete coating will reduce the sensors selectivity while an unnecessary thick coating might reduce sensitivity and increase response times. It is generally accepted that efficient structural control at the nanoscale can only be achieved by "bottom-up" methods and that self-assembly processes will play a key role. Self-assembly processes are attractive as they allow us to control nanoscale features via convenient macroscopic control parameters such as concentration and temperature without direct intervention at the nanoscale.

* To whom correspondence should be addressed. E-mail: h.bock@hw.ac.uk.

Experimental investigation of the details of adsorption and self-assembly of amphiphilic molecules on CNTs is challenging and only a limited number of systematic stydies are available in the literature. For example, Utsumia et al.[11] and Matarredona et al.[12] studied adsorption of NaDDBS on single wall carbon nanotubes. Their experiments show that adsorption follows a two-step mechanism which is due to debundling of the CNTs. Detailed interpretation of the results is, however, difficult as no direct evidence of the adsorbed structures was available. Transmission electron microscopy was used by Richard et al.[13] to study aggregation of different surfactants on various CNT samples. They observed a wide range of adsorbed structures which were strongly dependent on the thermodynamic conditions. Shvartzamn et al.[14] used high sensitivity differential scanning calorimetry to study self-assembly of surfactants on CNTs. They found that the nanotube diameter has a great influence on the structure of the adsorbed phase.

Computer simulations are convenient tools to study amphiphilic self-assembly on CNTs as they allow us to investigate the thermodynamics of self-assembly as well as the structure of the adsorbed phase within the same simulation framework, thus, avoiding the intrinsic experimental problem of observing the adsorbed structures. A number of methods, usually using a coarse-grained description, have successfully been employed to study adsorbed structures of amphiphilic and nonamphiphilic organic molecules on CNTs and other surfaces. Düren et al.[15] used grand canonical Monte Carlo simulations to study the adsorption of methane inside CNTs. Canonical Monte Carlo has been used to investigate the wrapping of polymers around CNTs in the work of Gurevitcha et al.[16] Nativ et al.[17] used classical molecular dynamics to study adsorption and aggregation of amphiphilic molecules on a single wall carbon nanotube (SWCNT). They found that adsorbed surfactant molecules cause a long ranged repulsive force between the nanotubes. This creates a repulsive barrier hindering rebundling of nanotubes. Qiao et al.[18] and Wallace et al.[19] used molecular dynamics to investigate the dependence of adsorbed structures on the bulk concentration and calculated the average orientation of the surfactant molecules with respect to the CNT-axis to characterize

10.1021/jp804891a CCC: $40.75 
Published on Web 10/15/2008

the structures. Dissipative particle dynamics (DPD) has successfully been used by Pastorino et al.[20] to investigate the properties of polymer brushes on planar surfaces.

In this paper we employ dissipative particle dynamics (DPD) simulations to study surfactant self-assembly from solution onto crossing single wall CNTs to understand self-assembly processes in materials comprising randomly arranged CNTs as the fundamental building blocks. We find that (i) self-assembly is directed to the nanotube/nanotube crossings due to a concentration of hydrophobic forces in these regions and (ii) self-assembly can be controlled efficiently by the concentration of the amphiphiles.

**Model and Simulation.** ***Model.*** In this paper, we employ computer simulations to study self-assembly of amphiphilic molecules in bulk solution and on carbon nanotubes. In the simulations surfactant molecules are represented by a chain of beads ($H_5T_5$) consisting of a block of five hydrophilic head (H) beads and a block of five hydrophobic tail (T) beads while the solvent is considered implicitly. The implicit treatment of the solvent as well as the coarse-grained character of the surfactant beads causes the beads to interact via effective potentials. In the present case we employ a common empirical model where the interactions between a pair of hydrophobic beads is attractive, while all other bead/bead interactions are repulsive. Attractive interactions between beads $i$ and $j$ are represented by the pair potential $\phi(r_{ij})$ which is based on the force shifted Lennard-Jones (LJ)(12,6) potential

$$\phi_{LJ}(r_{ij}) = 4\epsilon\left[\left(\frac{\sigma}{r_{ij}}\right)^{12} - \left(\frac{\sigma}{(r_{ij} - r_{cut})}\right)^{6}\right] \quad (1)$$

$$\phi(r_{ij}) = \begin{cases} \phi_{LJ}(r_{ij}) - \phi_{LJ}'(r_{cut})r_{ij} - \phi_{LJ}(r_{cut}) & r_{ij} < r_{cut} \\ 0 & r_{ij} \geq r_{cut} \end{cases} \quad (2)$$

where $\phi_{LJ}'(r) = d\phi_{LJ}(r)/dr$ and $r_{cut}$ is the cutoff-radius. In eq 1, $r_{ij} = ||\mathbf{r}_{ij}||$, $\mathbf{r}_{ij} = \mathbf{r}_j - \mathbf{r}_i$, and $\mathbf{r}_i$ and $\mathbf{r}_j$ are the positions of $i$ and $j$, respectively; $\epsilon$ is the well depth and $\sigma$ the length parameter of the LJ potential. Repulsive interactions are represented by the Weeks−Chandler−Anderson (WCA) potential given by eq 2 with $r_{cut} = 2^{1/6}$. For simplicity, these interactions are assumed to be present between all pairs of beads regardless whether they are bonded or not. In addition, two beads $k$ and $l$ which are nearest neighbors in a single surfactant chain interact via the harmonic bond potential

$$\phi_{bond}(r_{kl}) = \epsilon_{bond}(r_{kl} - r_{bond})^2 \quad (3)$$

where $\epsilon_{bond}$ is the depth of the potential well and $r_{bond}$ the bond length. Superposition of the nonbonding interaction and the harmonic bond potential with $\epsilon_{bond} = 4\epsilon$ and $r_{bond} = 1.2\sigma$ (Table 1) leads to an average nearest neighbor H/H distance of $1.35\sigma$ and a T/T distance of $1.26\sigma$. Thus, surfactant molecules are represented by a not too loose chain of beads.

At the length scale of the coarse-grained surfactant beads, the atomistic structure of the nanotubes becomes (essentially) irrelevant and surfactant beads interact with the mean-field of the nanotube. Therefore, we model the nanotubes as smooth cylinders. They interact with the hydrophobic surfactant beads via the force shifted Lennard-Jones (12,6) potential in eq 2 which is also shifted to the surface of the nanotubes

$$\phi_{CNT}(r_i) = \frac{\epsilon_{CNT}}{\epsilon}\phi(r_i - r_{CNT}) \quad (4)$$

where $r_i$ is the shortest distance between bead $i$ and the nanotube axis (for the formula see, e.g., ref 21) and $r_{CNT}$ is the radius of the nanotube. Interactions of the hydrophilic head beads with the nanotubes are modeled using the WCA potential, i.e., $\phi_{CNT}(r_i)$ with $r_{cut} = 2^{1/6}$. All potential parameters can be found in Table 1.

**TABLE 1: Model and Simulation Parameters in Reduced Units[a]**

| | |
|---|---|
| **Surfactants** | |
| T beads = 5 | H beads = 5 |
| $\epsilon = 1.0$ | $\sigma = 1.0$ |
| $\epsilon_{bond} = 4.0$ | $\sigma_{bond} = 1.2$ |
| **Nanotubes** | |
| $r_{CNT} = 1.0$ | $d_{CNT} = 3.0$ |
| $\theta_{CNT} = \pi/2$ | $\epsilon_{CNT} = 1.5$ |
| **Simulation** | |
| $T = 0.7$ | $\Delta t = 0.005$ |
| attractive: $r_{cut} = 2.5$ | repulsive: $r_{cut} = 2^{1/6}$ |
| nonconservative: $r_{cut} = 2.5$ | DPD: $\xi = 1.0$ |
| **Simulation Bulk** | |
| chains = 500 | cubic box = variable dimensions |
| equilibration = $1 \times 10^8\Delta t$ | production = $0.5 \times 10^8\Delta t$ |
| **Simulation Adsorption** | |
| chains = variable | elongated box = $100 \times 100 \times 200$ |
| equilibration = $(1-2) \times 10^8\Delta t$ | production = $0.5 \times 10^8\Delta t$ |

[a] $d_{CNT}$ is the distance and $\theta_{CNT}$ is the angle between nanotubes.

While the present model has been widely used, two specific features, i.e., the form and especially the well depth of the interaction between surfactant beads and the nanotubes, deserve a more detailed discussion. For this interaction we assume a LJ (12,6) potential because of its simple mathematical form and because it describes the actual physical situation well. Single wall carbon nanotubes consist of a single layer of carbon atoms located on the surface of a cylinder. Mean-field approximation for the interaction of a single LJ particle with a single planar layer of LJ particles leads to a (10,4) potential.[22] Because of the curvature of the cylinder the mean-field potential is slightly steeper in the case of CNTs (see ref 23 for the formal prove and ref 24 for an approximation). Thus, the resulting potential is very similar to a LJ (12,6) potential. Moreover, Patel et al. have fitted an LJ (12,6) potential to the potential of mean force between a carbon nanotube and methane ($CH_4$) molecules obtained from MD simulations and found excellent agreement.[25] The latter result is of particular relevance as it includes also the hydrophobic interaction. Thus, at the level of detail considered here the LJ (12,6) potential is a very reasonable choice.

As the focus of this paper is to investigate adsorption and aggregation of surfactant molecules on CNTs it is important to use a value for the ratio $\epsilon_{CNT}/\epsilon$ that is realistic and could be reproduced experimentally. The bead/bead interaction consists of at least two parts: the van der Waals interaction and the (effective) hydrophobic interaction, and is usually vastly dominated by the hydrophobic part. Calculations using the potential form of ref 24 reveal that for typical single wall carbon nanotubes with radii of a few nm the well depth of the van der Waals bead/nanotube interaction is approximately 2.7 times deeper than that of the bead/bead interaction. To estimate the ratio of the strength of the hydrophobic part of the bead/nanotube and that of the bead/bead interaction we estimate the ratio of the excluded surface areas. As a crude approximation it can be assumed that the strength of the hydrophobic interaction between two hydrophobic particles depends linearly on the size of the surface area that becomes unavailable to the solvent upon contact of the particles.[26] In the present case of spherical beads and cylindrical nanotubes, we find a ratio of the bead/nanotube to the bead/bead hydrophobic interaction of approximately 1.37(see appendix). If we assume that the hydrophobic interaction contributes 90% of the total interaction[27] we find $\epsilon_{CNT}/\epsilon \approx 1.5$.

Our model, which is empirical and contains no fitted parameter, is also validated by comparison with experiments. The model predicts that the ratio between the critical surface aggregation concentration and the cmc $C_{csac}/C_{cmc} \approx 0.3$. Matarredona et al. have measured NaDDBs adsorption on CNTs from aqueous solution and find $C_{csac}/C_{cmc} \approx 0.1$[12] which is in reasonable agreement with our results. It is also important to realize that one has some control over the strength of the van der Waals and the hydrophobic interaction in practice. The van der Waals interactions can be altered by altering the chemistry of the surfactants while the hydrophilicity of the solvent can be controlled using cosolvents (see, e.g., ref 28).

***Simulation.*** We investigate the system in the canonical ensemble using the dissipative particle dynamics (DPD) method.[29] In DPD two particles $i$ and $j$ interact via the pairwise force

$$F_{ij} = F_{ij}^{C} + F_{ij}^{R} + F_{ij}^{D} \tag{5}$$

where $F_{ij}^{C}$, $F_{ij}^{R}$, and $F_{ij}^{D}$ are the conservative, the random and the dissipative force, respectively.

The conservative force acts along the line connecting $i$ and $j$, $\hat{\mathbf{r}}_{ij} = \mathbf{r}_{ij}/|\mathbf{r}_{ij}|$, and depends only on the distance $r_{ij}$ between $i$ and $j$. It is given by the first derivative of the interaction potentials discussed above

$$F_{ij}^{C} = \begin{cases} -[\phi'(r_{ij}) + \phi'_{bond}(r_{ij})]\hat{\mathbf{r}}_{ij} & \text{nearest neighbors} \\ -\phi'(r_{ij})\hat{\mathbf{r}}_{ij} & \text{else} \end{cases} \tag{6}$$

The random force

$$F_{ij}^{R} = \begin{cases} -\xi\omega^{R}(r_{ij})\theta_{ij}\hat{\mathbf{r}}_{ij}\dfrac{1}{\sqrt{\Delta t}} & r_{ij} \le r_c \\ 0 & r_{ij} > r_c \end{cases} \tag{7}$$

represents forces from the (rapidly moving) degrees of freedom which have been coarse-grained out, such as collisions with solvent particles leading to Brownian motion of solutes. In DPD these forces are assumed to be pairwise and random in strength. In eq 7, $\Delta t$ is the simulation time step, $\xi$ is a parameter determining the maximal strength of the random force, $\omega^{R}(r_{ij})$ is a weight function characterizing its distance dependence and $\theta_{ij}$ is a random variable with zero mean and unit variance (see ref 30 for the random number generator we are using for our long trajectories). As the conservative force, the random force acts along the line connecting $i$ and $j$.

The dissipative force (or drag force)

$$F_{ij}^{D} = \begin{cases} -\gamma\omega^{D}(r_{ij})(\hat{\mathbf{r}}_{ij} \cdot \mathbf{v}_{ij})\hat{\mathbf{r}}_{ij} & r_{ij} < r_c \\ 0 & r_{ij} > r_c \end{cases} \tag{8}$$

represents the viscous drag mediated by degrees of freedom which have been coarse-grained out. In eq 8, $\gamma$ is the strength parameter and $\omega^{D}(r_{ij})$ is the weight function of the dissipative force. It is a pairwise force acting along the line connecting the interacting particles $i$ and $j$ and it reduces the relative velocity (component along $\hat{\mathbf{r}}_{ij}$) $\hat{\mathbf{r}}_{ij} \cdot \mathbf{v}_{ij}$, where $\mathbf{v}_{ij} = \mathbf{v}_j - \mathbf{v}_i$ and $\mathbf{v}_i$ and $\mathbf{v}_j$ are the velocities of $i$ and $j$, respectively.

In the canonical ensemble the dissipative and the random force are not independent but connected by the fluctuation dissipation theorem leading to

$$\omega^{D}(r_{ij}) = [\omega^{R}(r_{ij})]^2$$
$$\xi^2 = 2\gamma k_B T \tag{9}$$

where $k_B$ is Botzmann's constant and $T$ is the temperature. Thus, the random and the dissipative forces together constitute the DPD thermostat. Here we use the weight functions originally published in ref 29

$$\omega^{D}(r_{ij}) = \begin{cases} (1 - r_{ij}/r_{cut})^2 & r_{ij} < r_{cut} \\ 0 & r_{ij} > r_{cut} \end{cases} \tag{10}$$

where we have chosen $\omega^{D}(r)$ to be of the same range as the attractive conservative force.

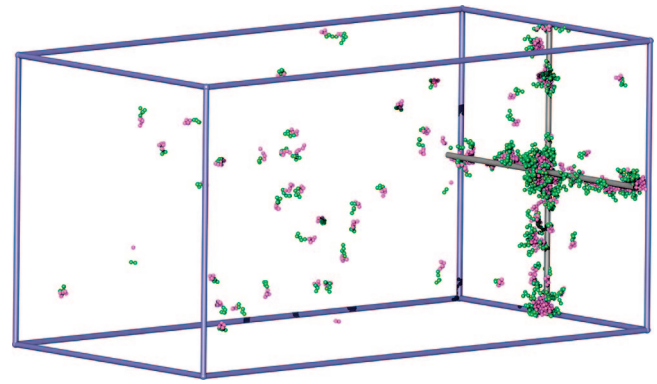

**Figure 1.** Elongated simulation box of size $100\sigma \times 100\sigma \times 200\sigma$. The CNTs are positioned on the far right side of the box and are partially covered with surfactant molecules. The usual periodic boundary conditions are applied in all three dimensions. Blue lines demarcate the simulation box.

In all simulations, we employ the usual periodic boundary conditions. Bulk simulations are carried out in a cubic simulation box while for the adsorption studies it is more convenient to use an elongated box that has the form of a quadratic prism (Figure 1). This allows us to study the adsorbed phase in equilibrium with a bulk (like) phase in the same system. We assume that at a distance of $30\sigma$ away from the nanotube the solution exhibits bulk properties as no correlations should be longer ranged. This is important as the bulk concentration is the key link to experiments.

For the adsorption simulations, it is convenient to be able to fix the bulk concentration. To achieve this, we perform chain insertions and deletions in the bulk-like region during the first half of the equilibration period, while in the second half the system is conventionally equilibrated in the canonical ensemble by standard DPD. Every 300 timesteps insertions or deletions are attempted if the actual concentration deviates from the target concentration by +5% or −5%, respectively. Insertion is accepted if none of the beads of the new molecule interacts with any existing chain. If this is not the case the insertion trial is repeated at different locations until it is successful. The acceptance probability is usually very high since the (bulk) concentration is very low.

The nanotubes are placed on one side of the box (Figure 1). They are rigid and their position is fixed. Since the tubes are not allowed to move they interact with the surfactant molecules only via the conservative part of the force.

$$F_i^{CNT} = \phi'_{CNT}(r_i) \tag{11}$$

Simulations are very long $\geq 10^8$ timesteps. The equilibration period of each simulation is determined individually by visual inspection of the evolution of relevant data, such as the concentration of free chains, the number of adsorbed chains etc. This is necessary as equilibration times can vary significantly around the cmc and the csac. Equilibration periods are typically $1-2 \times 10^8$ time steps in the bulk and $10^8$ steps for adsorption studies, while production runs are generally $0.5 \times 10^8$ time steps.

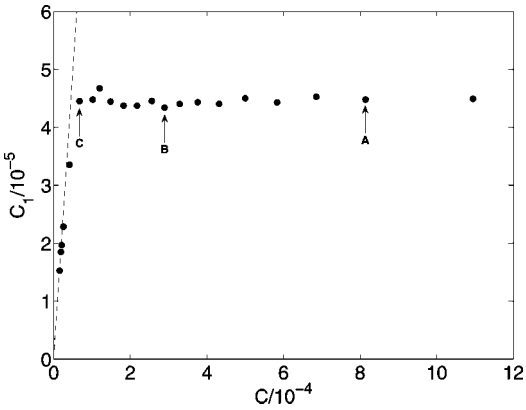


**Figure 2.** Concentration of free surfactant molecules $C_1$ versus the total concentration of surfactant molecules $C$. The dashed line demarcates $C_1 = C$ and the arrows indicate data points for which aggregation number distributions are shown in Figure 4.

In the bulk as well as on surfaces, surfactant molecules self-assemble into clusters and aggregates (e.g., micelles). We define that two molecules belong to the same cluster if any intermolecular tail-tail distance is smaller than $1.5\sigma$,[31] that is, the hydrophobic parts of the molecules are in close proximity. To identify all clusters a depth-first-search (DFS) algorithm is used (see, e.g., ref 32). We define a molecule as adsorbed if the distance between any of its tail beads and the axis of the nanotube is smaller than $1.5\sigma+r_{CNT}$.

***Reduced Units.*** Throughout we use reduced quantities: all length are given in units of the LJ length parameter $\sigma$, the energy scale is given in units of the well depth of the bead/bead LJ interaction $\epsilon$, the temperature scale is given in terms of $\epsilon/k_B$ where $k_B$ is the Boltzmann constant, and time is represented in units of $[m\sigma^2/\epsilon]^{1/2}$, where $m$ is the mass of a bead. Concentrations are defined as number (of molecules) densities and given in units of $1/\sigma^3$.

## II. Results and Discussion

**A. The Bulk Solution.** In bulk solutions, surfactant molecules form well defined aggregates at some threshold concentration called critical micelle concentration (cmc). The cmc depends on the surfactant and the solvent as well as on the thermodynamic conditions. Since our model is empirical and coarse-grained, it does not represent one particular experimental solvent/surfactant combination but it describes the generic behavior of all these systems. In order to link our results to the behavior of a specific surfactant and solvent, thermodynamic reference points are needed. The most relevant reference point for self-assembly is the cmc. Therefore we carefully determine the cmc and relate all other results to it.

The cmc indicates the surfactant concentration at which aggregation becomes relevant in the system. We can determine the cmc by plotting the concentration of free surfactant molecules $C_1$ as a function of the total surfactant concentration $C$ (figure 2). At low concentrations no aggregates are formed and, thus, $C_1 = C$. When micelles appear the concentration of free surfactant molecules must be smaller than the total concentration as some surfactant molecules are now bound in micelles. At this point $C_1(C)$ falls below the line $C_1 = C$. After a certain "transition region" one usually observes $C_1 \approx$ const. This is easily observed in Figure 2.

As micelle formation is a continuous process, there is some arbitrariness in the definition of the cmc. Here we define the cmc as the center between the last data point which approximately follows $C_1 = C$ and the first point which belongs to the group of points for which $C_1 \approx$ const. Thus for the present system we find $C_{cmc} = 5.2 \times 10^{-5}$.

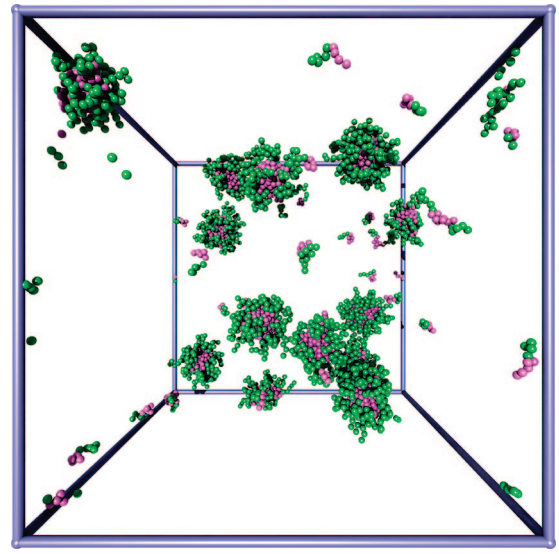

**Figure 3.** Snapshot of the system at $C = 8.2 \times 10^{-4} \approx 16C_{cmc}$. Hydrophilic beads are shown in purple while hydrophobic beads are colored green. The system contains mostly micelles and only very few free surfactant molecules. The blue frame indicates the simulation box.

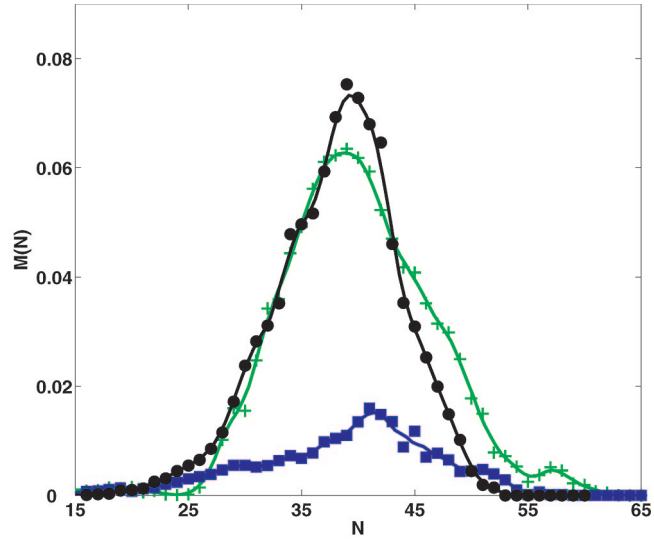


**Figure 4.** Cluster size distributions as probability mass functions for three surfactant concentrations $C = 6.70 \times 10^{-5}$ (blue ■), $C = 2.89 \times 10^{-4}$ (green +), and $C = 8.12 \times 10^{-4}$ (black ●) labeled in Figure 2 as A, B, and C, respectively. While the number of aggregates in the system increases with increasing concentration, the mean aggregation number remains constant.

The snapshot in Figure 3 gives an impression of the system at $C = 8.2 \times 10^{-4}$ which is well above the cmc. As expected, at this concentration the system is dominated by micelles of approximately spherical shape which are similar in their physical size. From detailed inspection of the snapshots, we can obtain a crude estimate of the diameter $d$ of the hydrophobic core of the micelles. At the present concentration $C = 8.2 \times 10^{-4}$, we find $d \approx 4.8$. We have also checked that the physical size of the micelles is very similar for all concentrations above the cmc used in this study.

The observation of similar physical size of the micelles is corroborated by the aggregation number distributions shown in Figure 4 where we plot the "probability mass function"

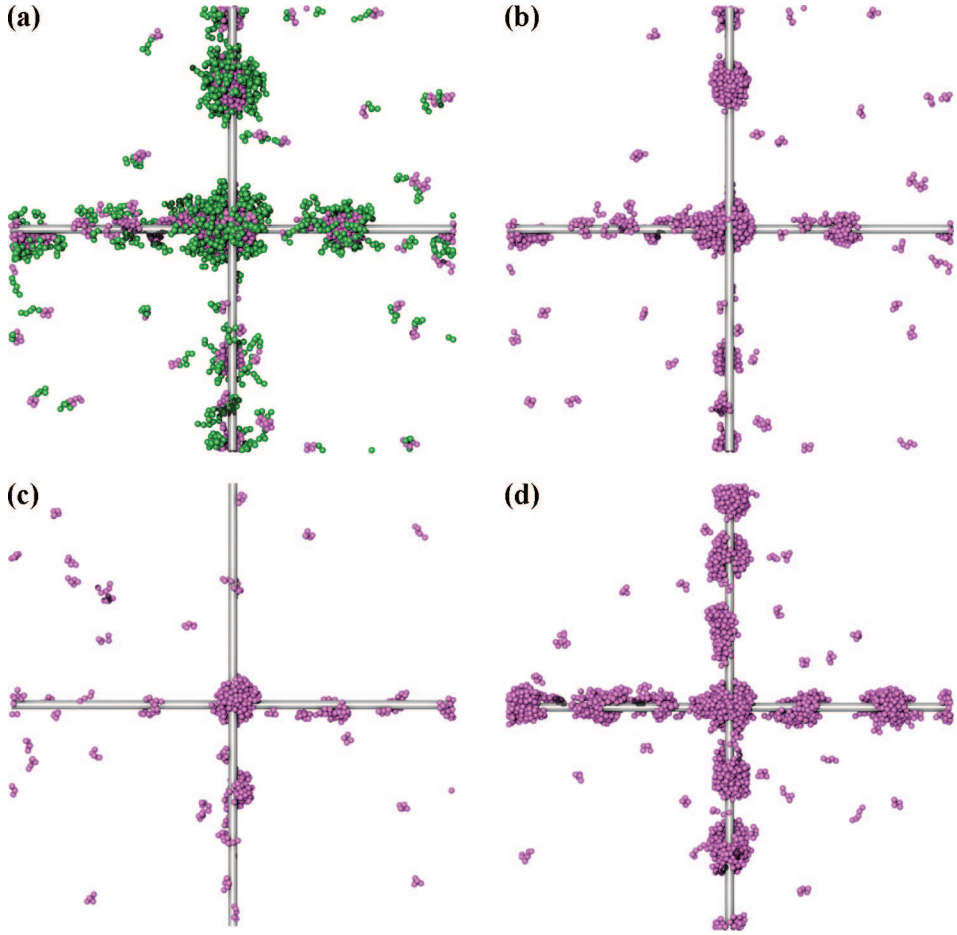


**Figure 5.** Simulation snapshots at various concentrations as indicated in the figure: (a) depicting the hydrophilic surfactant head groups in green and the hydrophobic tails in purple and (b−d) showing only the hydrophobic tails. In snapshot (d) the central aggregate is connected to the aggregate below and on the right via only very few molecules.

$$M(N) = \left\langle \frac{Nn_N}{\sum_{N=0}^{\infty} Nn_N} \right\rangle \tag{12}$$

where $N$ is the aggregation number of a cluster, $n_N$ is the number of clusters of size $N$ in the system and $\langle ... \rangle$ denotes the canonical ensemble average. $M(N)$ can be interpreted as the probability of finding a surfactant molecule in a cluster of aggregation number $N$. As can be inferred from the distributions in Figure 4, the aggregation numbers fluctuate around a mean value $\bar{N} = 40$ and, although the distributions have been obtained at significantly different concentrations, they all are relatively narrow and strikingly similar (except in magnitude). This indicates that the system clearly prefers spherical micelles consisting of approximately 40 surfactant molecules at all concentrations shown in Figure 4.

**B. Surfactant Adsorption and Aggregation on Crossing Carbon Nanotubes.** The central goal of this work is to investigate how surfactant molecules adsorb and aggregate in the heterogeneous environment formed by crossing carbon nanotubes and to what extent this can be controlled by the (bulk) surfactant concentration. In the snapshot taken at a concentration of $C = 1.59 \times 10^{-5}$ and presented in Figure 5, panels a and b, we observe a number of adsorbed molecules, small clusters and larger clusters which appear to be self-assembled aggregates. One aggregate, which we call the "central aggregate", is located at the nanotube crossing. It seems to be slightly larger in size and to contain more molecules than the others. It also appears to be symmetric, winding around the crossing rather than covering it completely. The other aggregates on the nanotubes seem to be radially asymmetric (with respect to the tube axis) and attach to the nanotubes sidewise rather than enclosing them. This closely resembles hemimicelles which are known to form on planar hydrophobic surfaces.[33]

More detailed information is provided by the cluster size distributions presented in Figure 6. Here the cluster size distribution is defined as the (canonical ensemble average of the) probability that a certain adsorbed cluster has an aggregation number $N$

$$P(N) = \left\langle \frac{n_N}{\sum_{N=0}^{\infty} n_N} \right\rangle \tag{13}$$

Note that this is different compared to the probability mass function used in Figure 4. To compute the cluster size distribution of the central aggregate $P_c(N)$, we define a cluster to be adsorbed at the nanotube crossing if at least one of its molecules is adsorbed on one of the nanotubes no further than $0.5\sigma$ away from the crossing (Figure 7).

As the plot in Figure 6a shows, $P_c(N)$ is approximately bell shaped with a maximum at $N_c^{max} \approx 48$ and, due to the symmetry of $P_c(N)$, the average aggregation number $\bar{N}_c = 48$, which is about 20% larger than the average size of a micelle in the bulk solution (above the cmc). Adsorption energy seems to stabilize the larger aggregate. However, there appears to be a limit to the possible size increase. It is at first surprising that the crossing is not fully enclosed by the central aggregate (Figure 5b)

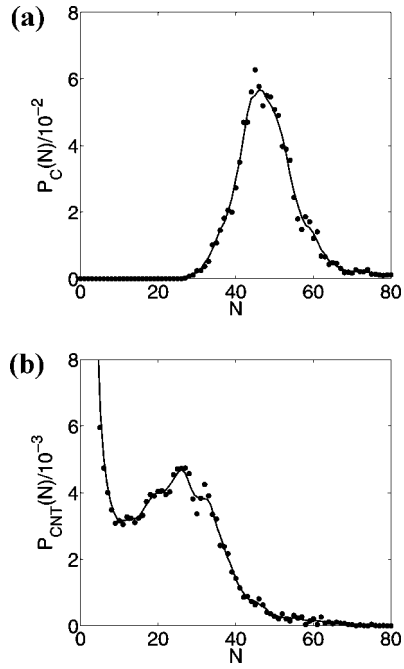


**Figure 6.** Cluster size distributions at $C = 1.59 \times 10^{-5}$: (a) for the central aggregate $P_c(N)$ and (b) for all adsorbed clusters excluding the central aggregate $P_{CNT}(N)$.

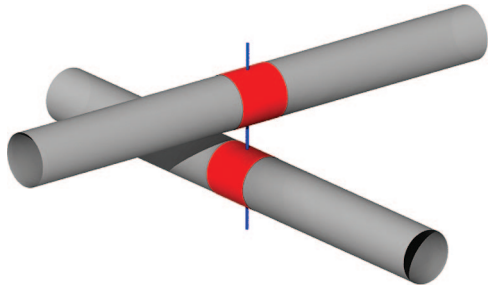

**Figure 7.** A cluster is defined to be adsorbed at the nanotube crossing if one of its molecules is adsorbed within the $1.0\sigma$ long nanotube section (indicated in red) which is centered at the center of the crossing (demarcated by the blue line).

although full enclosement would increase the adsorption energy. On the other hand it is well-known that the size (and shape) of micelles in bulk solution is determined by the curvature of the interface between the hydrophobic micellar core and its hydrophilic surrounding. This preferred curvature originates from the space requirements of the surfactant tails and heads. These distinct space requirements also exist in the case where surfactant molecules are adsorbed although altered by the interaction with the substrate(s). Even in the present case of adsorption and aggregation at the nanotube crossing with its large surface area and its very heterogeneous interaction potential the size of the aggregate seems to be largely determined by the surfactants rather than by the surface. This observation indicates that size and shape of adsorbed surfactant aggregates might be predictable based on their bulk counterparts which would represent an important tool for the rational design of nanostructured materials.

The cluster size distribution $P_{CNT}(N)$ of aggregates adsorbed along the nanotubes (not including the central aggregate) presented in Figure 6b is distinctly different compared to the central aggregate. We observe adsorption of single molecules and small clusters. Their probability decreases quickly with increasing size. Before the probability reaches zero, however,

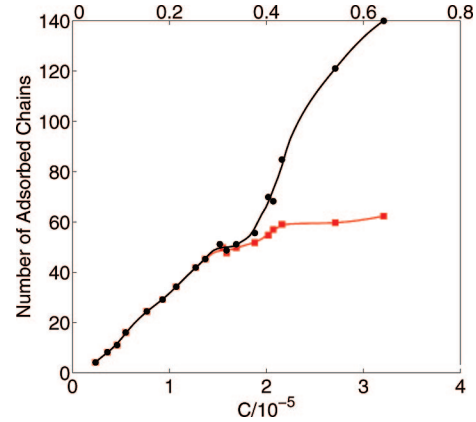


**Figure 8.** Number of surfactant molecules adsorbed at the CNT crossing $\bar{N}_c'$ (●) and the number of chains in the central aggregate defined via the first peak of the cluster size distribution $\bar{N}_c$ (■) as a function of (bulk) concentration. See text for details.

we observe a pronounced shoulder with a weak maximum indicative of surface aggregation. This behavior resembles the bulk solution, although in the adsorbed case $\bar{N}_{CNT} = 28$ is approximately 30% smaller than the average aggregation number in the bulk $\bar{N} = 40$ and the separation of small clusters from micelles is not as pronounced as in the bulk case, i.e., $P_{CNT}(N) > 0$ for all $N < \bar{N}_{CNT}$.

***1. The Central Aggregate.*** In the case discussed above, the central aggregate covers the nanotube crossing well while the rest of the tubes is not fully covered. This suggests that the higher hydrophobic potential at the nanotube crossing directs adsorption and self-assembly toward the crossing. This might offer the opportunity to control self-assembly in CNT materials.

The simplest control parameter known to influence adsorption from solution is the (bulk) concentration of surfactant molecules. As expected, the average number of surfactant molecules in the central aggregate $\bar{N}_c'$ increases with increasing (bulk) concentration (Figure 8). Furthermore, one immediately recognizes three distinct regions in $\bar{N}_c'(C)$: for $C \leq 1.5 \times 10^{-5}$, the aggregation number of the central aggregate increases (essentially) linearly, whereas in the concentration interval $1.5 \times 10^{-5} < C < 2.0 \times 10^{-5}$, we find only a weak increase. For $C \geq 2.0 \times 10^{-5}$ $\bar{N}_c'(C)$ again increases steeply.

To investigate the origin of this behavior we plot cluster size distributions for the central aggregate $P_c(N)$ at four different concentrations $C = 1.08 \times 10^{-5}$, $1.59 \times 10^{-5}$, $2.07 \times 10^{-5}$, and $2.71 \times 10^{-5}$ in Figure 9. It is striking that all cluster size distributions presented in Figure 9 reveal that the probability of finding a central aggregate of size $N = 0$, i.e., no central aggregate, is zero, from which we draw the important conclusion that the central aggregate is always present and only fluctuates in shape and size but never leaves the nanotube crossing. This is the case for all concentrations in Figure 8 except the two lowest $C = 0.24 \times 10^{-5}$ and $C = 0.36 \times 10^{-5}$ ($P_c(N)$ not shown).

At $C = 1.08 \times 10^{-5}$ $P_c(N)$ has a relatively sharp peak with $N_c^{max} \approx 31$ representing the central aggregate and is almost symmetric with the tendency of a slightly higher probability for clusters with $N > N_c^{max}$. This is consistent with the average cluster size of $\bar{N}_c' \approx 34$ (Figure 8) which is slightly larger than $N_c^{max}$.

As $C$ increases, the first peak in $P_c(N)$ shifts to larger aggregation numbers until $N_c^{max} \approx 55$ at which point any further increase of the concentration does not lead to any increase of $N_c^{max}$ suggesting that the central aggregate does not grow beyond

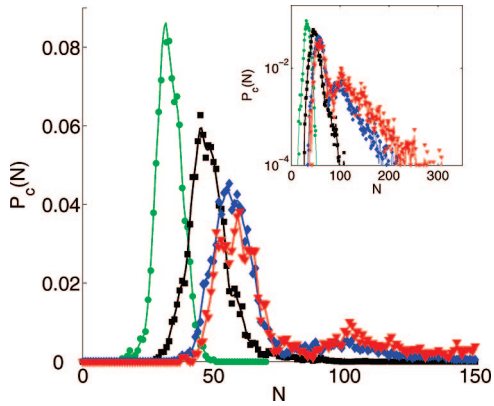


**Figure 9.** Cluster size distributions for the central aggregate $P_c(N)$ for four different concentrations $C = 1.08 \times 10^{-5}$ (green ●), $1.59 \times 10^{-5}$ (black ■), $2.07 \times 10^{-5}$ (blue ◇), and $2.71 \times 10^{-5}$ (red ∇). To emphasize the tails at large $N$, we replot the functions in a semilogarithmic plot in the inset.

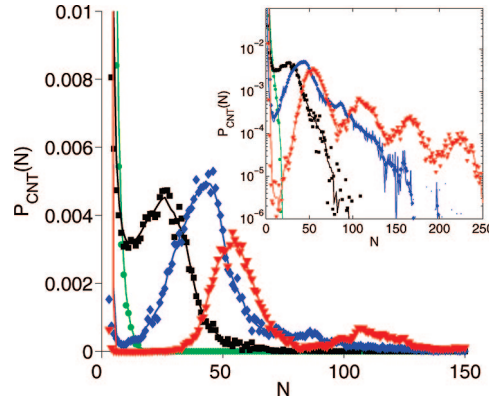


**Figure 10.** Cluster size distributions of adsorbed clusters (excluding the central aggregate) $P_{CNT}(N)$ for four different concentrations $C = 1.37 \times 10^{-5}$ (green ●), $1.59 \times 10^{-5}$ (black ■), $2.02 \times 10^{-5}$ (blue ◇), and $2.98 \times 10^{-5}$ (red ∇). To emphasize the tails at large $N$, we replot the functions in a semilogarithmic plot in the inset.

approximately 55 molecules. However, for $C > 1.59 \times 10^{-5}$ a new feature appears in $P_c(N)$, that is all cluster size distributions have a "tail". In the case of the two highest concentrations $2.07 \times 10^{-5}$ and $2.71 \times 10^{-5}$, this tail is very pronounced and shows a peak at $N \approx 100$. This peak is caused by aggregates (of approximately 45 molecules) which temporarily connect to the central aggregate rather than being incorporated. As all the concentrations in Figure 9 are well below the cmc, connecting clusters can not be located in the surrounding (bulk) solution but must be absorbed at the nanotube surfaces. Such a case is shown in the snapshot in Figure 5d (see also the Supporting Information).

According to our technical definition of the central aggregate, clusters temporarily connected to the central aggregate by even a single molecule are considered part of it leading to the large tail of $P_c(N)$ and $\bar{N}_c' > 55$. It seems, however, more sensible to redefine the central aggregate to be represented by the first peak of $P_c(N)$. This new definition leads to the mean aggregation number of the central aggregate $\bar{N}_c$ presented in Figure 8. Up to a concentration of $C \approx 1.5 \times 10^{-5}$ both $\bar{N}_c'$ and $\bar{N}_c$ coincide. At higher concentrations, where cluster size distributions show a tail, $\bar{N}_c$ falls below $\bar{N}_c'$ and shows little further increase. $\bar{N}_c$ levels off at approximately 55 molecules indicating that the central aggregate has reached a size limit beyond which it can not grow. This is caused by the tendency of the surfactant molecules to form spherical aggregates under the present thermodynamic conditions. The maximal mean aggregation number of the central aggregate $\bar{N}_c^{max} = 55$ is considerably larger than the average size of bulk micelles (beyond the cmc) $\bar{N}_{bulk} = 40$, but it appears that the adsorbed aggregate can not be very much larger than a bulk micelle. This might be a useful guide to choose a surfactant in practice.

***2. Adsorption and Aggregation on the Nanotubes.*** As the (bulk) surfactant concentration changes, both the amount of surfactant molecules adsorbed on the nanotubes and the structure they are forming change. This is shown in Figure 5 where we present representative snapshots at three concentrations $C = 1.37 \times 10^{-5}$, $1.59 \times 10^{-5}$, and $2.02 \times 10^{-5}$. At the lowest concentration shown ($C = 1.37 \times 10^{-5}$), we observe a relatively well developed central aggregate while only single molecules and small clusters are adsorbed elsewhere on the nanotubes. At $C = 1.59 \times 10^{-5}$, the adsorbed phase also consists of single molecules and small clusters but is dominated by larger (but still small) clusters of similar size which is indicative of aggregation. At the highest concentration $C = 2.02 \times 10^{-5}$, almost exclusively large aggregates are adsorbed, some of which seem to be connected to other aggregates and/or to the central aggregate. Since the aggregates occupy almost the entire nanotube surface there is very little space for movement. Because of the periodicity of the system (through the use of periodic boundary conditions) clusters are confined along the nanotubes by the central aggregate(s). It appears that 5 adsorbed aggregates fit well between the crossings on each nanotube (Figure 5d).

Cluster size distributions of adsorbed clusters (excluding the central aggregate) $P_{CNT}(N)$ defined according to eq 13 and shown in Figure 10 quantify this observation. The cluster size distributions are distinctly different compared to those of the central aggregate (Figure 9). At the lowest concentration $C = 1.37 \times 10^{-5}$ $P_{CNT}(N)$ shows that adsorbed molecules occur as individual molecules and small clusters with a quickly decaying probability at increasing size $N$.

At $C = 1.59 \times 10^{-5}$, the cluster size distribution has essentially the same features but it also shows a pronounced shoulder with a weak maximum at $N_{CNT}^{max} \approx 25$ which is a clear sign of aggregation.

Similar to the central aggregate, the cluster size distribution of adsorbed clusters shows a small tail with no particular structure. These tails can now be understood considering that $P_{CNT}(N)$ is largely dominated by (very) small clusters, i.e., adsorbed aggregates are separated along the tubes by individual adsorbed molecules and small clusters. Thus, it is more likely that the aggregates (temporarily) connect to these small clusters rather than to other aggregates. Since the probability of these small clusters decays quickly with increasing size the tail is short and has no maxima.

At all higher concentrations the situation is very different. The adsorbed phase is now clearly dominated by large aggregates. At $C = 2.02 \times 10^{-5}$, we find $N_{CNT}^{max} \approx 43$ and a second maximum in the tail at $N \approx 85$ while small clusters are almost completely absent. Because of the absence of small clusters aggregates are no longer separated by them and can temporarily connect to each other. At the same time the adsorbed aggregates now also connect to the central aggregate which explains the maximum at $N \approx 100$ in the tail of $P_c(N)$ at $C = 2.07 \times 10^{-5}$ shown in Figure 9. Animations of the system trajectories reveal that for concentrations $C > 2.0 \times 10^{-5}$ adsorbed clusters frequently connect and disconnect but rarely loose their identity (Supporting Information).

The results discussed above show that surfactant molecules readily adsorb on the nanotubes at concentrations well below

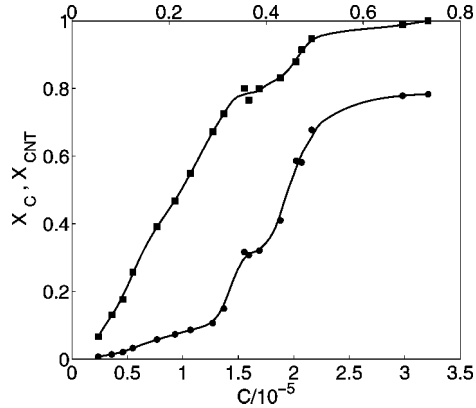


**Figure 11.** Coverage of the nanotube crossing (central aggregate) $X_c$ (●) (obtained from $N_c$ in Figure 8) and of the nanotubes not including the central aggregate $X_{CNT}$ (■) as a function of (bulk) concentration.

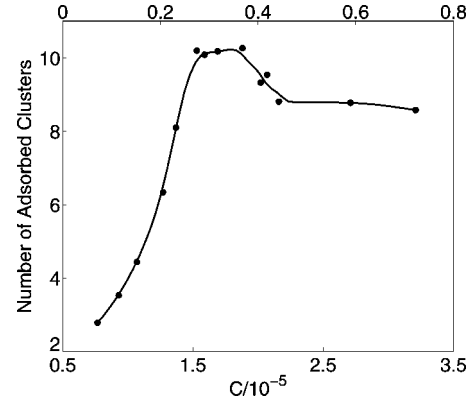


**Figure 12.** Number of adsorbed clusters (excluding the central aggregate) as a function of (bulk) concentration. Here we consider all clusters larger than dimers.

the cmc but prefer the nanotube crossing. This is quantified in Figure 11 where we compare the coverage of the nanotube crossing (central aggregate) $X_c$ and the coverage of the nanotubes (excluding the central aggregate) $X_{CNT}$ as a function of (bulk) concentration. Here coverage is defined as the ratio between the adsorbed amount at concentration $C$ and the amount adsorbed at a reference concentration $C = 7.6 \times 10^{-5}$. At this reference state we observe no noticeable increase in adsorption upon further increase of the (bulk) concentration, thus, we regard this state as "fully covered".

As expected, $X_c$ and $X_{CNT}$ increase with increasing concentration. Moreover, the results in Figure 11 clearly show that adsorption is directed toward the nanotube crossing. Thus, the nanotube crossing reaches full coverage well before the nanotubes are fully covered. This preferential adsorption is caused by the higher hydrophobic potential at the nanotube crossing due to the presence of two hydrophobic surfaces. Due to the preferential adsorption there is a concentration "window" $1.2 \times 10^{-5} \lesssim C \lesssim 1.7 \times 10^{-5}$ where the central aggregate is well developed while elsewhere the nanotube surfaces are relatively empty. This suggest that we have reasonable control over the adsorbed structures.

Besides these global features our results also provide very interesting insight into the details of the system's behavior. At $C \approx 1.5 \times 10^{-5}$ the coverage of the nanotubes $X_{CNT}$ shows a pronounced shoulder, which is also visible in the coverage of the crossing $X_c$. The steep increase of $X_{CNT}$ preceding the shoulder (Figure 11) in combination with the appearance of a maximum in the cluster size distributions at all concentrations $C > 1.5 \times 10^{-5}$ (Figure 10) suggest that the critical surface aggregation concentration (csac), the concentration where surface aggregation occurs in the system, is located at approximately $1.4 \times 10^{-5}$. Surface aggregation causes the coverage to increase quickly until saturation is reached, where it levels off.[40] At the csac aggregates of preferred size are formed (largely on the cost of adsorbed clusters). Thus, the adsorbed amount increases by increasing the number of aggregates (of preferred size) until the surface is saturated at which point no new aggregates can be formed.

This interpretation is corroborated by the results in Figure 12 where we plot the number of adsorbed clusters (not included in the central aggregate) as a function of (bulk) concentration. Here we consider all clusters which are larger than dimers. The number of adsorbed clusters initially grows with increasing concentration until it reaches a value of 10 at $C \approx 1.5 \times 10^{-5}$ just after the csac, thereafter it stays constant at 10. The slight decrease for $C > 2.0 \times 10^{-5}$ is caused by connecting clusters.

Increase of the bulk concentration beyond $1.5 \times 10^{-5}$ increases the driving force for adsorption. However, because no further aggregate can be adsorbed due to space limitations and because the adsorbed aggregates have already reached their preferred size, $X_{CNT}$ initially increases very little. Upon further increase of $C$ we observe an increase in $X_{CNT}$ (Figure 11) at a constant number of adsorbed aggregates (Figure 12). Thus, the increase of the adsorbed amount is due to growth of the aggregates which is corroborated by the cluster size distributions in Figure 10. This size increase is accompanied by a structural change from hemimicelles to full radially symmetric micelles.

The central aggregate also behaves in an interesting way. Up to $C \approx 1.5 \times 10^{-5}$ it grows almost linearly with the (bulk) concentration. Because there is very little adsorption elsewhere on the tubes in this regime the central aggregate is essentially independent. This changes at $C \approx 1.5 \times 10^{-5}$, after which the nanotubes are filled and there is exchange between the adsorbed aggregates which is suggested by the tails in the cluster size distributions. Thus, for concentrations larger than $1.5 \times 10^{-5}$ the central aggregate is no longer independent but a part of the adsorbed phase. This interpretation is supported by the observation that from this concentration on the behavior of the central aggregate is very similar to that of the other adsorbed aggregates: Initially we observe a range of very little further growth and subsequently all aggregates grow. The only difference is that the central aggregate reaches its maximal size well before the nanotubes are fully covered.

## III. Conclusions

We have used DPD simulations to study how surfactants adsorb on crossing carbon nanotubes and to what extent this adsorption and the adsorbed structures can be controlled by the bulk surfactant concentration. Computer simulations are well suited for these investigations as they allow us to study the thermodynamics of surfactant adsorption as well as structural details of the systems within the same simulation framework.

Our key finding is that adsorption is directed to the nanotube crossing due to its higher hydrophobic potential. Adsorbed surfactant molecules form a central aggregate which is somewhat bigger and slightly distorted but otherwise similar to a bulk micelle. In particular, we find that it has a maximal size and can not grow much beyond the size of a bulk micelle. This strongly suggests that the properties of the central aggregate are influenced by the nanotube crossing but are dominated by the aggregation properties of the surfactant molecules. In the present case, bulk micelles are slightly smaller than the crossing,

thus, one would expect the central aggregate to cover the crossing only imperfectly which is indeed the case. From these results we draw the conclusion that (i) aggregation is directed to the nanotube crossing and (ii) it should be possible to estimate the size and shape of the central aggregate from the properties of bulk micelles.

Surfactant molecules also adsorb on the nanotubes outside the central aggregate but the coverage always lags behind that of the crossing, i.e. at lower concentrations the central aggregate forms and at higher concentrations surfactant molecules adsorb everywhere. At the critical surface aggregation concentration (csac) of $C_{csac} \approx 1.4 \times 10^{-5}$ adsorption is associated with surface aggregation. We find that a fixed number of aggregates forms on the nanotubes which does not increase any further upon increase of the bulk concentration. Instead, the surface aggregates grow in aggregation number whereby their shape transforms from hemimicelles to full micelles. From these results we conclude that (iii) we can control the structure of the adsorbed phase (to a certain degree) via the bulk surfactant concentration

**Acknowledgment.** This work was financially supported by an EPSRC DTA award and the Chemical Enginering Endowment Fund.

## Appendix A: Estimate of the Hydrophobic Interactions

As a crude estimate, it can be assumed that the surface energy of the interface between a hydrophobic solute and a hydrophilic solvent scales linearly with the solvent accessible surface area (sasa), that is the surface area that is available to the solvent (e.g., water). If two hydrophobic solute particles come near each other, the sasa decreases, resulting in a free energy reduction of the system which causes the effective attraction we call "hydrophobic interaction". If we further assume that the surface energy is dominated by water and depends little on the specific hydrophobic surface, the strength of the hydrophobic interaction between two hydrophobic solutes is roughly proportional to the reduction in the sasa upon their contact.

For the present study, we need to determine the ratio of the hydrophobic interaction between two hydrophobic surfactant beads and that between a hydrophobic bead and a CNT. According to the discussion above this ratio is identical to the ratio of the excluded solvent accessible surface areas (xsasa). In order to calculate this we need to specify some of the length scales in the system. For the present estimate we assume a single wall CNT with a diameter of 1nm and water molecules to have a radius of 0.16nm. The diameter of a surfactant bead in our model (Table 1) is half the diameter of the nanotubes, thus, 0.5 nm. The xsasa for two spherical surfactant beads can be calculated analytically,[34] whereas we obtain the xsasa of the bead/nanotube contact via Monte Carlo integration. From these calculations, we estimate the ratio of the hydrophobic bead/bead and the hydrophobic bead/nanotube interactions to be approximately 1.37.

**Supporting Information Available:** This information is available free of charge via the Internet at http://pubs.acs.org.

## References and Notes

(1) Koziol, K.; Vilatela, J.; Moisala, A.; Motta, M.; Cunniff, P.; Sennett, M. *Science* **2007**, *318* (5858), 775–778.

(2) Vigolo, B.; Pnicaud, A.; Coulon, C.; Sauder, C.; Pailler, R.; Journet, C.; Bernier, P.; Poulin, P. *Science* **2000**, *290* (5495), 1331–1334.

(3) Motta, M.; Li, Y.-L.; Kinloch, I.; Windle, A. *Nano Lett.* **2005**, *5* (8), 1529–1533.

(4) Lee, S. W.; Kim, B.; Lee, D. S.; Lee, H. J.; Park, J. G.; Ahn, S. J.; Campbell, E. E. B.; Park, Y. W. *Nanotech.* **2006**, *17* (4), 992–996.

(5) Berhan, L.; Yi, Y. B.; Sastry, A. M.; Munoz, E.; Selvidge, M.; Baughman, R. *J. Appl. Phys.* **2004**, *95* (8), 4335–4345.

(6) Coleman, J. N.; Blau, W. J.; Dalton, A. B.; Munoz, E.; Collins, S.; Kim, B. G.; Razal, J.; Selvidge, M.; Vieiro, G.; Baughman, R. H. *Appl. Phys. Lett.* **2003**, *82* (11), 1682–1684.

(7) Schadler, L. S.; Giannaris, S. C.; Ajayan, P. M. *Appl. Phys. Lett.* **1998**, *73* (26), 3842–3844.

(8) Wall, A.; Coleman, J. N.; Ferreira, M. S. *Phys. Rev. B* **2005**, *71* (12),

(9) Johnson, A. T. C.; Staii, C.; Chen, M.; Khamis, S.; Johnson, R.; Klein, M. L.; Gelperin, A. *Semicond. Sci. Technol.* **2006**, *21* (11), S17–S21.

(10) Chen, R. J.; Bangsaruntip, S.; Drouvalakis, K. A.; Wong, N.; Kam, S.; Shim, M.; Li, Y.; Kim, W.; Utz, P. J.; Dai, H. *Proc. Natl. Acad. Sci. U.S.A.* **2003**, *100* (9), 4984–4989.

(11) Utsumi, S.; Kanamaru, M.; Honda, H.; Kanoh, H.; Tanaka, H.; Ohkubo, T.; Sakai, H.; Abe, M.; Kaneko, K. *J. Colloid Interface Sci.* **2007**, *328* (1), 276–284.

(12) Matarredona, O.; Rhoads, H.; Li, Z.; Harwell, J. H.; Balzano, L.; Resasco, D. E. *J. Phys. Chem.* **2003**, *107*, 13357–13367.

(13) Richard, C.; Balavoine, F.; Schultz, P.; Ebbesen, T. W.; Mioskowski, C. *Science* **2003**, *300* (5620), 775–778.

(14) Shvartzman-Cohen, R.; Florent, M.; Goldfarb, D.; Szleifer, I.; Yerushalmi-Rozen, R. *Langmuir* **2008**, *24* (9), 4625–4632.

(15) Düren, T.; Keil, F. J. *Chem. Eng. Technol.* **2001**, *24* (7), 698–702.

(16) Gurevitcha, I.; Srebnik, S. *Chem. Phys. Lett.* **2007**, *444* (1−3), 96–100.

(17) Nativ-Roth, E.; Shvartzman-Cohen, R.; Bounioux, C.; Florent, M.; Zhang, D.; Szleifer, I.; Yerushalmi-Rozen, R. *Macromolecules* **2007**, *40* (10), 3676–3685.

(18) Qiao, R.; Ke, P. C. *J. Am. Chem. Soc.* **2006**, *128* (42), 13656–13657.

(19) Wallace, E. J.; Sansom, M. S. P. *Nano Lett.* **2007**, *7* (7), 1923–1928.

(20) Pastorino, C.; Kreer, T.; Müller, M.; Binder, K. *Phys. Rev. E* **2007**, *76*, 026706−026716.

(21) Weisstein E. W.;"Point-Line Distance--3-Dimensional." From MathWorld---A Wolfram Web Resource. http://mathworld.wolfram.com/Point-LineDistance3-Dimensional.html.

(22) Desai, T.; Keblinski, P.; Kumar, S. K. *Polymer* **2006**, *47*, 722.

(23) Kirsch, V. A. *Adv. Colloid. Interface* **2003**, *104*, 311–324.

(24) Tanaka, H.; El-Merraoui, M.; Steele, W. A.; Kaneko, K. *Chem. Phys. Lett.* **2002**, *352*, 334–341.

(25) Patel, N.; Egorov, S. A. *J. Am. Chem. Soc.* **2005**, *127* (41), 14124–14125.

(26) Lee, B.; Richards, F. M. *J. Mol. Biol.* **1971**, *55* (3), 379–400.

(27) Leckband, D.; Israelachvili, J. *Q. Rev. Biophys.* **2001**, *34* (02), 105–267.

(28) Lin, Y.; Alexandridis, P. *Langmuir* **2002**, *18*, 4220–4231.

(29) Groot, R. D.; Warren, P. B. *J. Chem. Phys.* **1997**, *107* (11), 4423–4435.

(30) Matsumoto, M.; Nishimura, T. *ACM Trans. Model. Comput. Simul.* **1998**, *8* (1), 3–30.

(31) von Gottberg, F. K.; Smith, K. A.; Hatton, A. T. *J. Chem. Phys.* **1997**, *106* (23), 9850–9857.

(32) Cormen, T. H.; Leiserson, C. E.; Rivest, R. L.; Stein C. *Introduction to Algorithms*, 2nd ed.; The MIT Press: Cambridge, MA, 2001.

(33) Grant, L. M.; Ducker, W. A. *J. Phys. Chem. B* **1997**, *101* (27), 5337–5345.

(34) Wodak, S. J. J.; Janin, J. *April* **1980**, *77* (4), 1736–1740.

(35) Stone, J. *An Efficient Library for Parallel Ray Tracing and Animation*; Master's thesis, 1998.

(36) Humphrey, W.; Dalke, A.; Schulten, K. *J. Mol. Graphics* **1996**, *14*, 33–38.

(37) Shinto, H.; Morisada, S.; Higashitani, K. *J. Chem. Eng. Jpn.* **2005**, *38* (7), 465–477.

(38) Yerushalmi-Rozen, R.; Szleifer, I. *Soft Matter* **2006**, *2* (1), 24–28.

(39) Shvartzman-Cohen, R.; Nativ-Roth, E.; Baskaran, E.; Levi-Kalisman, Y.; Szleifer, I.; Yerushalmi-Rozen, R. *J. Am. Chem. Soc.* **2004**, *126* (45), 14850–14857.

(40) Note that we are well below the cmc thus the "levelling-off" is not related to the bulk cmc as it is in many other cases.

JP804891A